On the Development of Optical Properties during Thermal Coarsening of Gold Nanoparticle Composites.

Shirin R. King, Angus R. Gentle, Michael B. Cortie and Andrew M. McDonagh*

Institute for Nanoscale Technology, University of Technology Sydney, PO Box 123, Broadway, NSW 2007, Australia

KEYWORDS: gold nanoparticles, sintering, stabilizing ligand, optical properties

ABSTRACT: The changes in optical properties that occur as gold nanoparticles (AuNPs) are thermally converted to a continuous thin film were studied with the purpose of determining the roles of particle coarsening and temperature. *In situ* reflectance spectroscopy, electron microscopy and synchrotron X-ray diffraction were applied to provide complementary information on the changes in particle size and shape. The AuNPs studied were stabilized with 1-butanethiol, 1-octanethiol, oleylamine or 4-(pyren-1-yl)butane-1-thiol. Initially the films were dark brown or purple in color, due to the plasmon resonance of the AuNPs. As the temperature was increased the AuNPs started to coalesce and percolate, thereby changing the color of the films to that of bulk gold. Films of AuNPs stabilized with alkanethiols sintered very rapidly, measured as a rapid change in the reflectance spectrum. In contrast, films of AuNPs stabilized with oleylamine or 4-(pyren-1-yl)butane-1-thiol sintered more gradually and at a higher temperature. This permitted the transition to be studied in greater detail than for the alkanethiols. Red-shifted plasmon peaks and increased intensity in the reflectance data, and XRD and electron microscopy measurements, revealed that a prolonged process of nanoparticle coarsening occurred prior to sintering. The effect of temperature on the optical properties was isolated by monitoring samples as they cooled. The insulator-to-metal transition in these types of composites offers a very flexible platform for controlling spectral properties in the near-infrared region.

Introduction

The useful and tunable optical properties of gold nanoparticles (AuNPs) have attracted considerable attention from nanotechnology researchers.[1, 2] The size- and shape-dependent optical properties of AuNPs arise from a localized surface plasmon resonance (LSPR) – a collective oscillation of the gold's conduction electrons in response to certain wavelengths of incident light. In addition to the dependence of the LSPR frequency on the size and shape of the nanoparticles and the dielectric function of their immediate surroundings,[3] the LSPR of AuNPs also has some dependence on temperature. As the temperature is raised, the plasmon band red-shifts slightly as a result of thermal lattice expansion, which decreases the electron density and leads to the electrons resonating at a lower frequency.[4, 5] There is also significant broadening and decreased intensity of the plasmon band with increasing temperature, which has been attributed to increased electron-phonon scattering.[4] These effects are reversible and repeatable[4, 6] and are more pronounced for larger nanoparticles,[7] however they are only observed over a large temperature range, on the order of a few hundred degrees Celsius. Therefore in order to measure the LSPR temperature dependence without damaging the AuNPs, most studies have used AuNPs embedded within glass or silica, since colloidal solutions can only be monitored over a relatively small temperature range, and deposited films of AuNPs are prone to sintering at temperatures around 200 °C.[8, 9] This dependence of the LSPR on temperature has potential applications in, for example, the optical sensing of temperature and gas composition simultaneously in the harsh conditions of certain industrial processes.[10-12]

Several prior studies have investigated the effect of heating on the optical properties of AuNP thin films. Red- and blue-shifts in the LSPR peak wavelength were observed, depending on film thickness and temperature/annealing time, and these were irreversible upon cooling the films to room temperature. Some of the films used in these studies were too thin to become electrically percolating upon heating, but instead became rougher with the formation of relatively large, discrete islands of gold as the particles coalesced.

The coalescence and sintering of thicker films of AuNPs results in significant changes to their optical properties, with the films rapidly changing from the dark color of the nanoparticles to lustrous gold upon sintering[13] (here we use the definition of coalescence as the disappearance of the boundary between two contacting gold particles and a subsequent reduction of the total surface area,[14] and sintering to be temperature-induced coalescence of the gold particles below the melting point of gold[15]). The change in the optical properties is a result of the Drude response[16] of the electrically conductive gold film; the reflectivity in the near-infrared (NIR) region of the spectrum decreases with increasing wavelength for a film of separated particles, but

increases with wavelength when the particles coalesce and the film becomes electrically percolating.[17, 18] This can be detected in sintering studies as a dramatic increase in electrical conductivity.[13, 19]

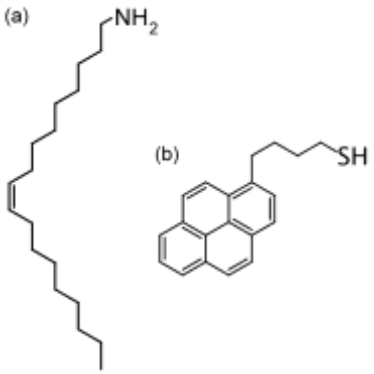

Figure 1. Structures of (a) oleylamine (OA) and (b) 4-(pyren-1-yl)butane-1-thiol (PyBuSH)

Recently we reported that certain organic compounds with high decomposition temperatures, such as oleylamine and 4-(pyren-1-yl)butane-1-thiol (Figure 1) can be used to stabilize films of AuNPs and delay the onset of sintering.[20] In addition to increasing the temperature of the sintering event (T_{SE}), these stabilizing compounds cause the sintering to progress far more gradually than has been observed for AuNPs stabilized with alkanethiols.[19] This prolonged sintering event provided us with a window to monitor the changes to the optical properties throughout the sintering process, and over a greater temperature range than would otherwise be possible with AuNPs of lower thermal stability. The results, reported herein, may have applications in sensors such as thermal history indicators for temperature sensitive materials or products.[21]

Experimental

General. Tetrachloroauric acid,[22] 1-butanethiol-capped AuNPs (BT@AuNPs),[23] 1-octanethiol-capped AuNPs (OT@AuNPs),[24] oleylamine-capped AuNPs (OA@AuNPs)[25] and 4-(pyren-1-yl)butane-1-thiol (PyBuSH)[20] were prepared using literature procedures. The functionalization of OA@AuNPs with PyBuSH (Py@AuNPs) has been described elsewhere.[20] The stabilizing compounds are reasonably transparent in the visible and NIR regions of the electromagnetic spectrum, and our previous work showed that oleylamine and PyBuSH greatly increase the thermal stability of AuNP films.[20] 1-Butanethiol and 1-octanethiol were included as comparators with low thermal stability.

Scanning electron microscopy (SEM) was performed using a Zeiss Supra 55VP SEM operating at 20 keV for samples drop cast onto silicon wafer. Transmission electron microscopy was conducted on a FEI Tecnai T20 TWIN microscope (LaB_6) operating at 200 keV and fitted with a Gatan 894 2k × 2k camera. All TEM samples were drop cast from toluene onto lacy carbon grids.

Optical measurements. UV-visible spectroscopy was performed using an Agilent Technologies Cary 60 UV-Visible spectrophotometer for samples dissolved in toluene, and an Agilent Technologies Cary 7000 Universal Measurement spectrophotometer for sample films on glass. Transmission, reflection and absorption were calculated using the Maxwell-Garnett effective medium approximation for a 30% volume fraction of gold spheres in air as a 20 nm thick film on glass.

The reflectance spectra of thin films of AuNPs were measured *in situ* in air whilst the temperature of the specimens was increased. Suspensions of AuNPs in chloroform were drop cast onto clear white glass slides. The apparatus consisted of an Ocean Optics LS-1 tungsten halogen light source and a USB-2000 Si photodiode array spectrophotometer with 5 mm diameter collimating and 25 mm diameter collection lenses (Ocean Optics 84-UV-25), leading to a 10 mm diameter sampling area. The light source and detector were each positioned at 15° either side of normal incidence to the sample. A sputtered aluminum reference mirror was used for calibration of the spectrometer. The sample was placed on a computer-controlled heating stage within the spectrometer, allowing reflectance spectra to be collected as the sample was heated at a rate of 10 °C min^{-1}. A LabVIEW program was used to synchronize sample heating and the collection of reflectance data. The reflectance spectra were measured at 6 s intervals. The data were then exported in a text format for post-processing and analysis.

Reflectance spectra were converted to CIE $L^*a^*b^*$ colors using the appropriate ASTM standard.[26] This scheme is adapted to the sensitivity of the average human eye such that a color distance of 1 unit is just detectable. L (luminance) indicates how bright the color is, a^* parameterizes the green to red components, and b^* the blue to yellow components. A coordinate of (0,0,0) is absolute black and (100,100,100) is pure white. Bulk gold has an a^* coordinate of between 4 and 12 (depending on surface texture) while b^* is usually about 35 to 40. The conversion from CIE $L^*a^*b^*$ to RGB and the colors appearing in the printed version of this paper are approximate only.

X-ray diffraction experiments. X-ray diffraction (XRD) studies on the OA@AuNPs were performed on the Powder Diffraction beamline at the Australian Synchrotron. A wavelength of 0.5900 Å was used, calibrated using a LaB_6 standard. A Mythen strip detector with 0.004°angular resolution was used. Samples were placed in 0.3 mm diameter SiO_2 capillaries and spun in a Eurotherm hot air blower and heated at 10 °C min^{-1}. Data were collected in 30 s segments with an intervening dead time of 12 s between segments due to the need to reposition the detector. Peak parameters were extracted from selected reflections by fitting a pseudoVoight peak onto a cubic background. Instrumental broadening was established as a function of 2θ using the LaB_6 standard and varied between 0.01° at low 2θ to 0.04° at 2θ=50°. Crystallite sizes and microstrain were extracted using a Williamson-Hall analysis after subtracting the instrumental broadening.

Results and Discussion

Table 1. AuNP characterization data.

	Particle Diameter (nm)	LSPR peak (nm)
BT@AuNPs	2–5	–
OT@AuNPs	5	518
Py@AuNPs	2–6	530
OA@AuNPs	2–6	524

Characterization data for the AuNPs used in this work are collected in Table 1. The synthesized BT@AuNPs were 2–5 nm in diameter and as described in our previous work.[8, 20, 27] The dark brown color of the colloid and the lack of a plasmon peak in the visible region (Supporting Information, Figure S1) are consistent with AuNPs on the size threshold for the emergence of localized surface plasmon resonance (LSPR).[28] The OT@AuNPs were reasonably monodisperse at ~5 nm in diameter (Supporting Information, Figure S2), with a plasmon resonance peak at 518 nm (Supporting Information, Figure S1). Py@AuNPs were prepared by introducing PyBuSH to a solution containing OA@AuNPs with no resultant change in particle size (Supporting Information, Figure S3).

OA@AuNPs were 2–6 nm in diameter,[20] (Supporting Information, Figure S4a). Measurement of the particle sizes from SEM images indicated that most of the particles were about ~5 nm in diameter and, as for OT@AuNPs and Py@AuNPs, this included a contribution from the shell of the stabilizing ligands. TEM images (Supporting Information, Figure S3b were analyzed to provide a more accurate measurement of the Au core and yielded an average particle diameter of 3.3 nm (Supporting Information, Figure S3c). These particles produced a deep red colloid and a plasmon resonance peak at 524 nm (Supporting Information, Figure S1).

Figure 2 shows *in situ* reflectance data for a film of OT@AuNPs upon heating, both as a function of wavelength (Figure 2a) and as a function of temperature (Figure 2b). The initial reflectance of the film was low, with a plasmon resonance peak at ~600 nm. This peak in the reflectance represents only a small component of the LSPR of the particles; a larger resonance peak would be observed if measuring transmission or absorption (Figure S5). The plasmon resonance peak of AuNPs in the film is red-shifted compared to that of the colloidal suspension (518 nm), which is caused by complex electromagnetic interactions between AuNPs that are in close proximity (but not touching).[29-31] The spectra remained largely unchanged up to ~220 °C. Between 226 and 228 °C the reflectance rapidly increased, particularly in the NIR region, indicating that the film had rapidly percolated to become electrically conductive.[18] The resulting spectrum was similar to the reflectance spectrum of bulk gold[32] (Supporting Information, Figure S6) but not as bright because the reflectance on the present samples has a diffuse characteristic. It is clear that sintering had occurred. The reflectance spectra collected during the heating of a film of BT@AuNPs (Supporting Information, Figure S7) follow a very similar trend to those of OT@AuNPs, but with the sharp increase in reflectance occurring at a lower temperature of 160 °C, as expected for AuNPs stabilized with a shorter alkanethiol.[13, 20, 33] The alkanethiol-stabilized AuNPs sinter too rapidly for any detailed information on the optical properties and structural changes that occur during the sintering process to be acquired. A system with a more gradual onset of percolation is required if details of the transient properties are desired.

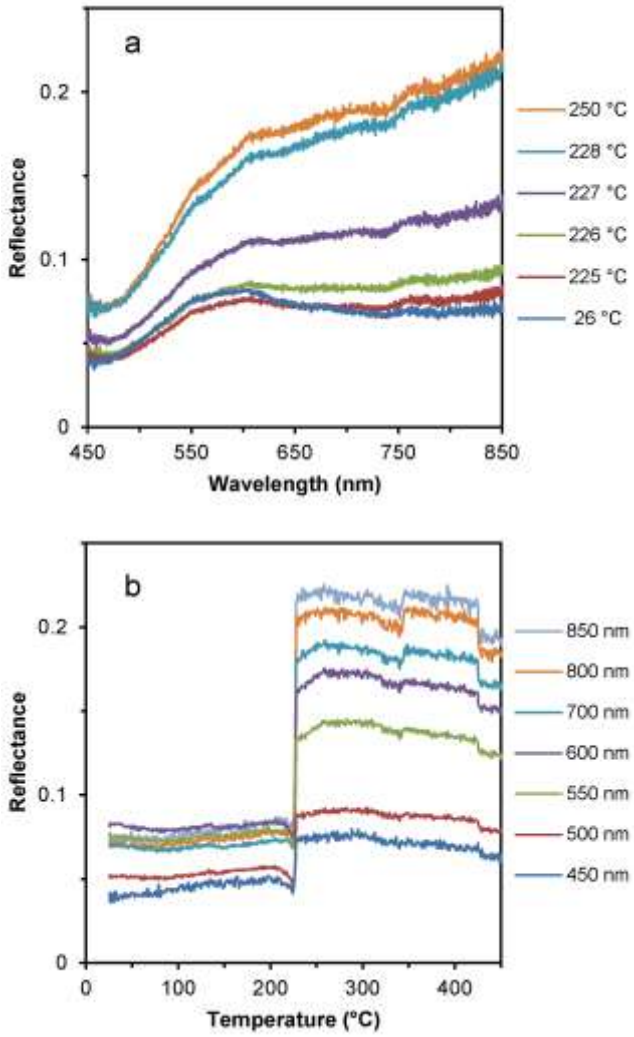

Figure 2. Raw reflectance data obtained from a film of OT@AuNPs during heating: (a) as a function of wavelength and (b) as a function of temperature.

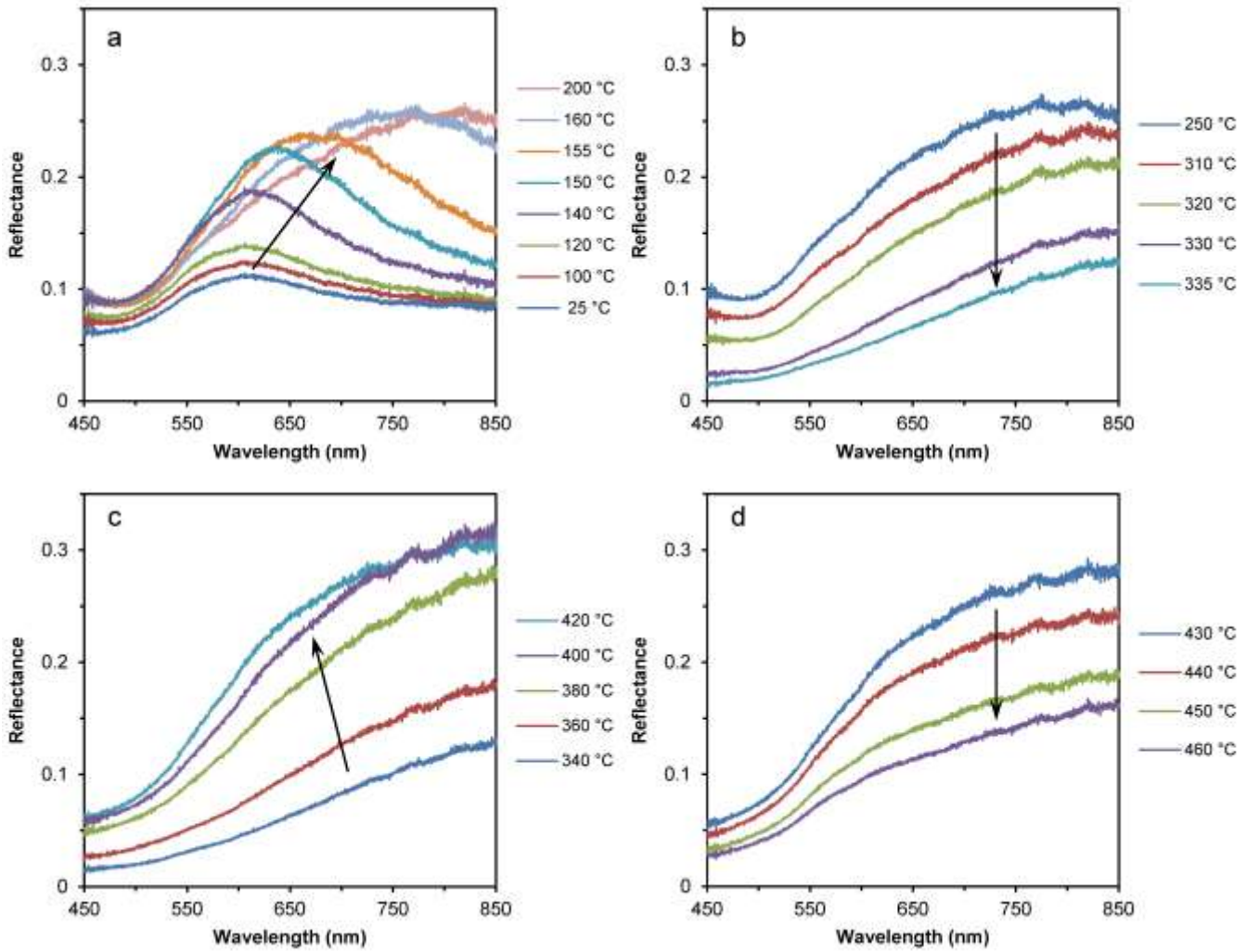

Figure 3. Raw reflectance spectra obtained from a film of Py@AuNPs during heating, separated into selected temperature ranges: (a) 25–200 °C, (b) 250–335 °C, (c) 340–420 °C and (d) 430–460 °C.

Py@AuNPs have much greater thermal stability than BT@AuNPs and OT@AuNPs, with a T_{SE} as high as ~390 °C.[20] In addition, the sintering event occurs over a significantly wider temperature range, on the order of ~100 °C.[20] The reflectance data collected while heating a film of Py@AuNPs are shown in Figure 3 and Figure S10 of the Supporting Information. A plasmon resonance peak was initially observed at ~600 nm (Figure 3a). The spectra remained unchanged up to ~80 °C, then between 80 and 200 °C the reflectance of the plasmon peak significantly increased and red-shifted to ~800 nm (Figure 3a). Importantly, this trend suggests that the Py@AuNPs are coarsening (that is, the larger particles draw material from the smaller particles, which is energetically favorable due to the very high surface energy of the smaller particles) without sintering. This is supported by the decreasing NIR reflectance with increasing wavelength at 200 °C, which indicates the film was not conductive.[17] The phenomenon of gold nanoparticle coarsening and migration on solid surfaces has been described[34, 35] with both of these processes observed at temperatures similar to those in the current work. There was very little change in the spectra from 200 to 250 °C, but between 250 and 335 °C the reflectance of the film significantly decreased across the spectrum (Figure 3b). This decrease is likely due to changes in the optical properties of the PyBuSH stabilizer as it decomposes (which occurs within this temperature range)[20] such as a darkening of the color and roughening of the texture, causing less light to be reflected, which was observed during the heating of a related compound, 1-pyrenebutanol (PyBuOH, Supporting Information, Figure S11). The NIR reflectance also increased at longer wavelengths between 250 and 335 °C (Figure 3b), suggesting that the gold crossed the percolation threshold to become conductive, which is expected to coincide with the decomposition of the stabilizing compound. Between 340 and 420 °C, the reflectance of the film greatly increased (Figure 3c) until the spectrum resembled that of bulk gold, which is attributed to the removal of the PyBuSH and its decomposition by-products and the consequent development of the gold into a more continuous film. Decreasing reflectance between 430 and 460 °C (Figure 3d) is attributed to the breaking up of the gold film into discrete islands.[36]

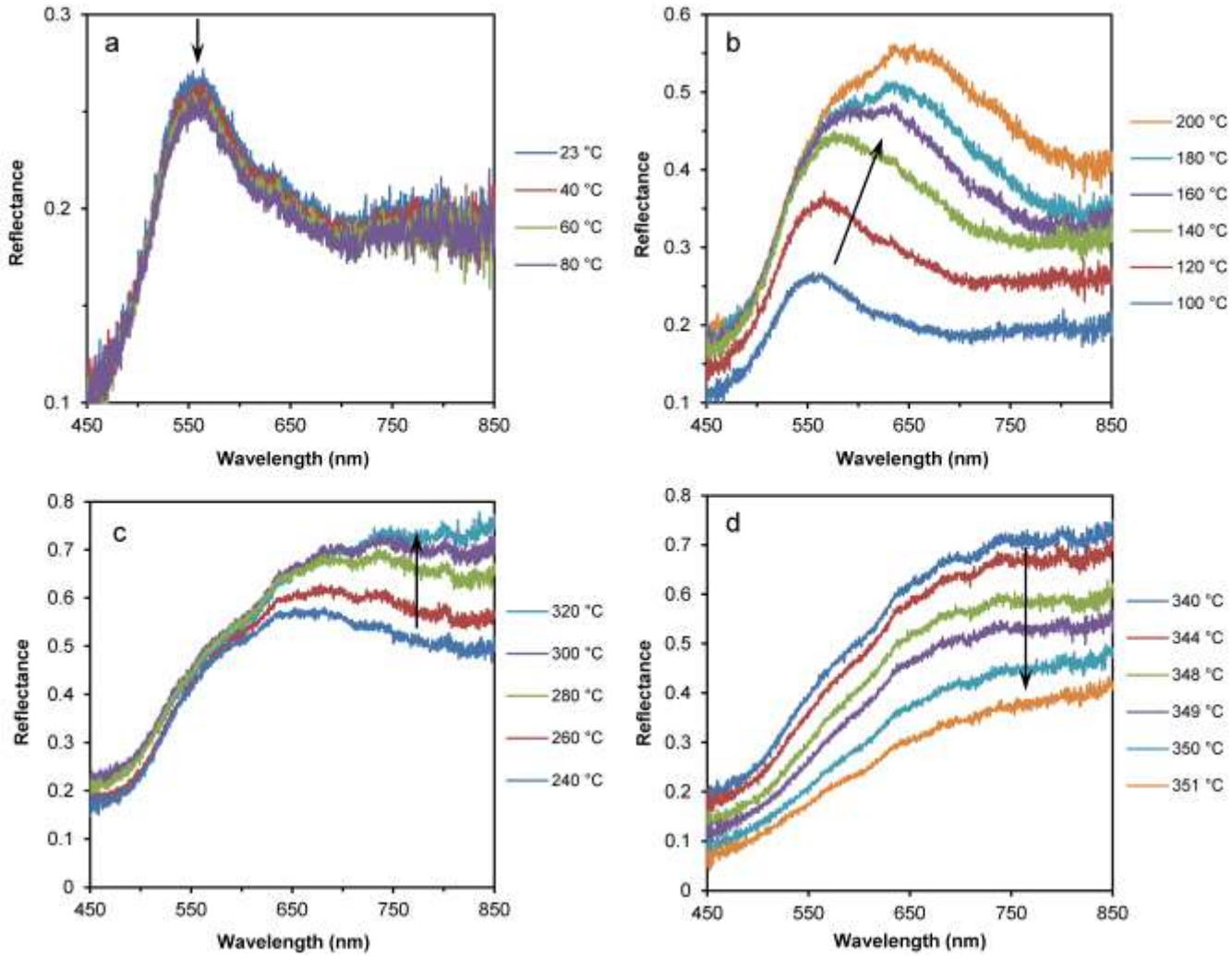

Figure 4. Raw reflectance spectra obtained from a film of OA@AuNPs during heating, separated into selected temperature ranges: (a) 23–80 °C, (b) 100–200 °C, (c) 200–340 °C and (d) 340–351 °C.

The reflectance data for a film of OA@AuNPs during heating are shown in Figure 4 and Supporting Information, Figure S9. We have previously shown films of OA@AuNPs to have a relatively high T_{SE} of ~320 °C.[20] Reflectance at 23 °C (Figure 4a) was low and a plasmon resonance peak was observed at ~546 nm, with an associated reflectance of 27%. Heating to 100 °C caused a slight decrease in the plasmon peak amplitude, consistent with literature describing the temperature dependence of the LSPR of AuNPs.[4, 5] Heating from 100 to 200 °C (Figure 4b) resulted in a redshift of the plasmon peak and a more than doubling of its reflectance, along with a broadening of the spectrum. We attribute this change to coalescence of the AuNPs to form various configurations containing fused particles.[37, 38] Between 200 and 340 °C, the reflectance at wavelengths longer than 630 nm increased incrementally as more particles coalesced, with the film becoming fully sintered (and thus, conductive) by 320 °C (Figure 4c). The gradual change in reflectance is consistent with our reported electrical resistance data[20] for OA@AuNPs where the change in resistance decreases gradually in the temperature range ~260–350 °C with the maximum rate of change at ~320 °C. Upon heating the film above 340 °C, a decrease in reflectance across the whole spectrum was observed (Figure 4d).

Analysis of the particle film by SEM (Figure 5b) reveals the changes to the particle structure that correspond to the changes in optical properties (Figure 5c). Each SEM image in Figure 5 corresponds to a different specimen heated to the desired temperature before measurement. The specimen shown in Figure 5b at 25 °C has a lower coverage of AuNPs. At 25 °C, the OA@AuNPs were at their original size and shape (~5 nm diameter and spherical). By 135 °C the AuNPs began to coarsen, increasing in diameter to ~15–20 nm and the particles maintained a spherical shape; this corresponds to the increased reflectance measured at this temperature. Upon heating to 173 °C, the particles became

significantly larger in diameter and a number of different shapes (for example rods, hexagons, triangles) can be observed. The corresponding reflectance spectrum indicates that this film was not electrically conductive and thus the particles were still insulated from each other. The increasing degree of polydispersity causes a broadening of the plasmon resonance peak. At 295 °C the particles were only slightly larger than at 173 °C and with the same type of shapes present, though lower magnification SEM images show the development of microstructures in the film (Supporting Information, Figure S9). The significant increase in the NIR reflectance at 295 °C shows that the film is very close to the electrical percolation threshold.[17] At 472 °C, large islands of sintered gold are evident. The process of island formation (de-wetting) upon the annealing of thin metallic films has been examined in the literature,[36] and is driven by the kinetic process of surface energy minimization.[39] This breaking apart of the gold film into islands accounts for the measured decrease in reflectance across the spectrum after heating beyond 340 °C (Figure 4d).

The color changes associated with the various stages of heating may be visualized within the framework of the widely used CIE *L*a*b** color coordinates (Figure 5d). Generally, the development of the optical properties, and hence colors, during sintering depends on the thickness of the film. Sufficiently thick films evolve from the tarnished brass color of the nanoparticle composite to the bright yellow of bulk gold with a strong increase in luminance, as seen in the first half of the color strip in Figure 5d. However, after prolonged heating the film will break up into islands and the reflectance decreases again, indicated by a drop in the value of *L*, which can be seen as a darkening of the color in the second half of Figure 5d.

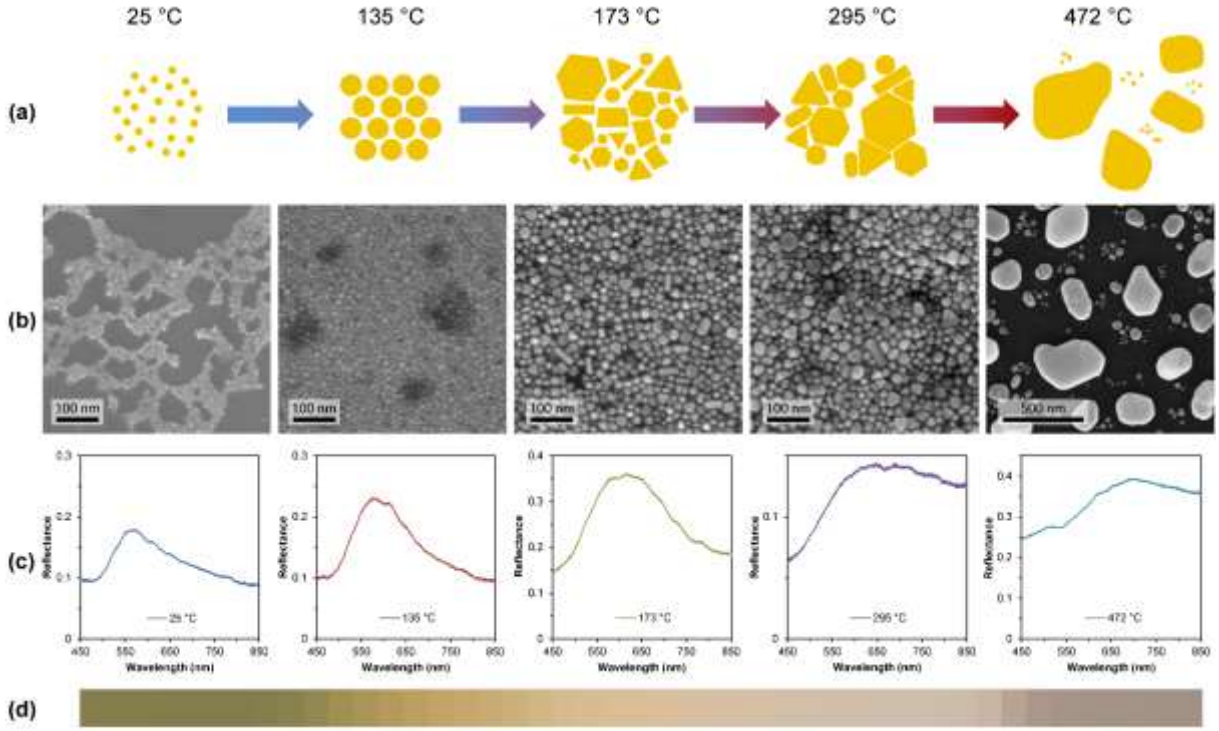

Figure 5. Particle structure and corresponding optical properties for films of OA@AuNPs heated from room temperature (left) to temperatures up to 472 °C (right): (a) illustrations showing particle morphology, (b) SEM images of the AuNP films after heating to each temperature, (c) optical reflectance spectra collected *in situ* (at temperature) for the films shown in (b), and (d) RGB colors recovered from the reflectance spectra of the film heated from room temperature to 472 °C using standard tables for CIE XYZ and CIE *L*a*b**.

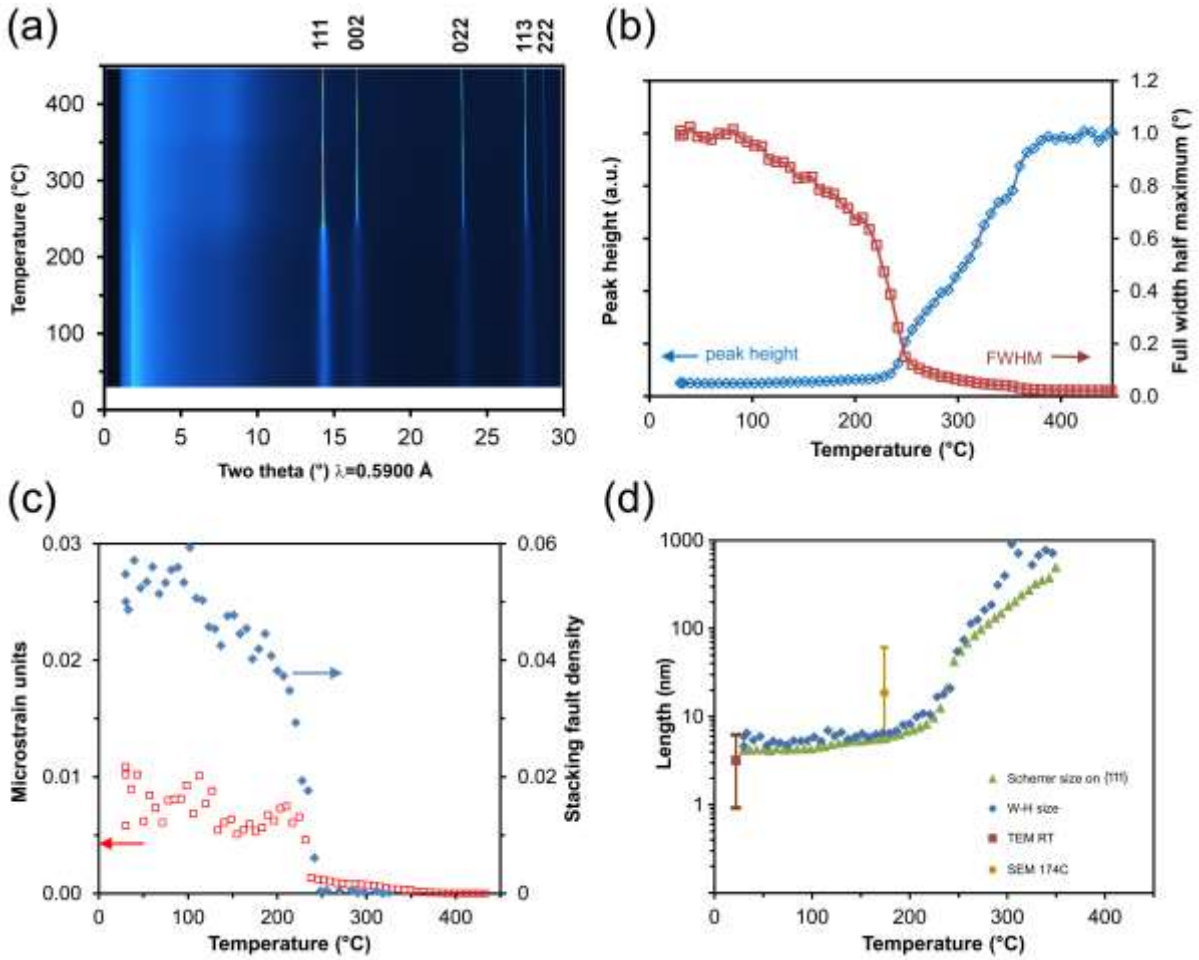

Figure 6. *In situ* synchrotron XRD data for heated OA@AuNPs (a) iso-intensity map showing formation of strongly crystalline peaks starting at ~230 °C, (b) variation of height and FWHM of the Au (111) peak, (c) variation of microstrain and stacking fault density, (d) crystallite sizes obtained from Scherrer analysis of the (111) peak, from a full Williamson-Hall (W-H) analysis, and the particle size determined by SEM.

Changes to particle structure upon heating were analyzed using *in situ* synchrotron X-ray powder diffraction. Figure 6a shows the development of the diffraction patterns in the form of an intensity map. The increase in the height and simultaneous decrease in width of the Au (111) peak is shown in Figure 6b (peak *area* is not shown as extraction of it was imprecise at the lower temperatures because of the acute sensitivity of such calculations to background noise and nature of analytical equation used.) The data show that the material recrystallized over the temperature range 240 to 360 °C. The crystallite size, microstrain and stacking fault density were extracted from the XRD data and are plotted in Figure 6c&d. In Figure 6d the average of the Scherrer size estimated from the (111) peak is plotted alongside a crystallite size estimated from a Williamson-Hall analysis of eight peaks. The XRD data indicate that the crystallites are of the order of 4–5 nm in size at the start of the heat treatment, in excellent agreement with the TEM results. In contrast, however, after the nanoparticles were raised to elevated temperature and then examined *ex situ* in SEM, the particle size becomes much larger than the crystallite size provided by XRD (the SEM estimate of particle size obtained at 174 °C is also shown in Figure 6d). We account this by noting that individual particles crystallized into more than one grain in many instances, either as separate crystals separated by a grain boundary, or as twins. This factor would produce an XRD crystallite size that is smaller than the physical particle size.

The XRD data for 3–4 nm diameter OA@AuNPs were collected from samples on a linear temperature ramp and so they cannot be directly compared to those obtained by Ingham *et al.*[40] using isothermal heat treatments applied to 10–12 nm diameter OA@AuNPs. However, in both cases very little change occurred up to about 170 °C, after which stacking faults began to anneal out. Our starting stacking fault density of about 0.05 is more than twice as high as the 0.02 reported by Ingham *et al.*, which is not unexpected considering that our nanoparticles were less than half the diameter and hence considerably more faulted. This latter aspect is also reflected in the microstrain of about 0.005 to 0.01 of our OA@AuNPs, which is high and much greater than the yield strain of annealed gold (E = 79 GPa, $\sigma_y \approx 75$ MPa, therefore $\varepsilon_y \approx 0.001$). This is the consequence of the fact that the crystalline lattice of these nanoparticles

is quite distorted relative to that of bulk gold. The interparticle scattering peak can also be observed in the X-ray pattern because it generates a low peak at a 2θ of about 1.85° but, due to this being at the limit of the instrument's range, no quantitative analysis was attempted. This peak disappears at 220–230 °C, suggesting that electrical percolation begins at this temperature.

Conclusions

Reflectance measurements of films of OA@AuNPs showed a gradual but significant red-shift in the LSPR peak wavelength and a more than doubling of its reflectance between 100 and 200 °C, which indicates a process of nanoparticle coarsening prior to sintering. This coarsening was confirmed by electron microscopy and XRD analyses, which revealed both an increase in particle size and a change in particle shape from spherical to a range of shapes such as rods, hexagons and triangles. Heating to 300 °C led to a change in the reflectance spectrum to resemble that of bulk gold as the particles sintered and the film became electrically conductive. Continued heating caused the film to undergo surface tension-driven island formation, resulting in a decrease in reflectance. Reflectance measurements of films of Py@AuNPs displayed similar characteristics to those of OA@AuNPs, though with some possible interference from the decomposition byproducts of the stabilizer. The dramatic changes in optical properties of these AuNP films over such a wide temperature range make them promising candidates as sensing materials in thermal history indicators.

The observations reported here were possible because of the sintering characteristics of the selected nanoparticles, which in turn are determined by the stabilizing ligands. AuNPs stabilized with 1-butanethiol or 1-octanethiol sinter very rapidly, which was measured here as sharp transition in the reflectance spectrum from that of a dark film of nanoparticles to a spectrum similar to that of bulk gold. In contrast, the sintering of AuNPs stabilized with PyBuSH or oleylamine proceeded much more gradually than the alkanethiol-stabilized AuNPs, and at a higher temperature, allowing the transitions to be studied in detail.

ASSOCIATED CONTENT

Supporting Information. UV-visible spectra, SEM and TEM micrographs, histogram of particle sizes for OA@AuNPs, photographs showing decomposition of PyBuOH. This material is available free of charge via the Internet at http://pubs.acs.org.

AUTHOR INFORMATION

Corresponding Author

Andrew.McDonagh@uts.edu.au

ACKNOWLEDGMENT

The authors thank D. Totonjian and K. McBean for assistance with electron microscopy, and the Australian Synchrotron for access to the Powder Diffraction Beamline. S.K. thanks the University of Technology Sydney for provision of a PhD scholarship.

REFERENCES

1. Amendola, V.; Pilot, R.; Frasconi, M.; Maragò, O. M.; Iatì, M. A., Surface Plasmon Resonance in Gold Nanoparticles: A Review. *J. Phys. : Condens. Matter* **2017,** *29*, 203002.

2. Daniel, M.-C.; Astruc, D., Gold nanoparticles: assembly, supramolecular chemistry, quantum-size-related properties, and applications toward biology, catalysis, and nanotechnology. *Chem. Rev.* **2004,** *104*, 293-346.

3. Kelly, K. L.; Coronado, E.; Zhao, L. L.; Schatz, G. C., The optical properties of metal nanoparticles: the influence of size, shape, and dielectric environment. *J. Phys. Chem. B* **2003,** *107*, 668-677.

4. Yeshchenko, O. A.; Bondarchuk, I. S.; Gurin, V. S.; Dmitruk, I. M.; Kotko, A. V., Temperature Dependence of the Surface Plasmon Resonance in Gold Nanoparticles. *Surf. Sci.* **2013,** *608*, 275–281.

5. Link, S.; El-Sayed, M. A., Size and Temperature Dependence of the Plasmon Absorption of Colloidal Gold Nanoparticles. *J. Phys. Chem. B* **1999,** *103* (21), 4212–4217.

6. Kreibig, U., Electronic Properties of Small Silver Particles: The Optical Constants and Their Temperature Dependence. *J. Phys. F Met. Phys.* **1974,** *4* (7), 999–1014.

7. Doremus, R. H., Optical Properties of Small Gold Particles. *J. Chem. Phys.* **1964,** *40* (8), 2389–2396.

8. Cortie, M. B.; Coutts, M. J.; Ton-That, C.; Dowd, A.; Keast, V. J.; McDonagh, A. M., On the coalescence of nanoparticulate gold sinter ink. *J. Phys. Chem. C* **2013,** *117* (21), 11377-11384.

9. Bishop, P. T.; Ashfield, L. J.; Berzins, A.; Boardman, A.; Buche, V.; Cookson, J.; Gordon, R. J.; Salcianu, C.; Sutton, P. A., Printed gold for electronic applications. *Gold Bull.* **2010,** *43* (3), 181-188.

10. Ohodnicki Jr., P. R.; Brown, T. D.; Holcomb, G. R.; Tylczak, J.; Schultz, A. M.; Baltrus, J. P., High Temperature Optical Sensing of Gas and Temperature Using Au-Nanoparticle Incorporated Oxides. . *Sensors Actuators B Chem.* **2014,** *202*, 489–499.

11. Ohodnicki Jr., P. R.; Wang, C.; Natesakhawat, S.; Baltrus, J. P.; Brown, T. D., In-Situ and Ex-Situ Characterization of TiO_2 and Au Nanoparticle Incorporated TiO_2 Thin Films for Optical Gas Sensing at Extreme Temperatures. . *J. Appl. Phys.* **2012,** *111* (6), 64311–64320.

12. Maurya, M. R.; Toutam, V., Size-Independent Parameter for Temperature-Dependent Surface Plasmon Resonance in Metal Nanoparticles. *J. Phys. Chem. C* **2016,** *120* (34), 19316–19321.

13. Huang, D.; Liao, F.; Molesa, S.; Redinger, D.; Subramanian, V., Plastic-compatible low resistance printable gold nanoparticle conductors for flexible electronics. *J. Electrochem. Soc.* **2003,** *150* (7), G412-G417.

14. Everett, D. H., *Manual of Symbols and Terminology for Physicochemical Quantities and Units. Appendix II*. Butterworths: London, 1971.

15. Alemán, J. V.; Chadwick, A. V.; He, J.; Hess, M.; Horie, K.; Jones, R. G.; Kratochvíl, P.; Meisel, I.; Mita, I.; Moad, G.; Penczek, S.; Stepto, R. F. T., Definitions of terms relating to the structure and processing of sols, gels, networks, and inorganic-organic hybrid materials (IUPAC Recommendations 2007). *Pure Appl. Chem.* **2007,** *79* (10), 1801-1829.

16. Dressel, M.; Scheffler, M., Verifying the Drude Response. *Ann. der Phys.* **2006,** *15* (7-8), 535-544.

17. Gadenne, P.; Beghdadi, A.; Lafait, J., Optical Cross-over Analysis of Granular Gold Films at Percolation. *Opt. Commun.* **1988,** *65* (1), 17-21.

18. Brandt, T.; Hövel, M.; Gompf, B.; Dressel, M., Temperature- and Frequency-Dependent Optical Properties of Ultrathin Au Films. *Phys. Rev. B* **2008,** *78* (20), 1-7.

19. Coutts, M.; Cortie, M. B.; Ford, M. J.; McDonagh, A. M., On the mechanism of sintering of thiol-stabilized gold nanoparticles: Formation of conductive gold films at room temperature. *J. Phys. Chem. C* **2009,** *113* (4), 1325-1328.

20. King, S. R.; Shimmon, S.; Totonjian, D. D.; McDonagh, A. M., Influence of Bound versus Non-Bound Stabilizing Molecules on the Thermal Stability of Gold Nanoparticles. *J. Phys. Chem. C* **2017,** *121* (25), 13944–13951.

21. Wang, Y. C.; Lu, L.; Gunasekaran, S., Biopolymer/gold Nanoparticles Composite Plasmonic Thermal History Indicator to Monitor Quality and Safety of Perishable Bioproducts. *Biosens. Bioelectron.* **2017,** *92* (June), 109-116.

22. King, S. R.; Massicot, J.; McDonagh, A. M. A., Straightforward Route to Tetrachloroauric Acid from Gold Metal and Molecular Chlorine for Nanoparticle Synthesis. *Metals* **2015,** *5* (3), 1454-1461.

23. Wu, Y.; Li, Y.; Liu, P.; Gardner, S.; Ong, B. S., Studies of gold nanoparticles as precursors to printed conductive features for thin-film transistors. *Chem. Mater.* **2006,** *18* (19), 4627-4632.

24. Yang, Y.; Yan, Y.; Wang, W.; Li, J., Precise Size Control of Hydrophobic Gold Nanoparticles Using Cooperative Effect of Refluxing Ripening and Seeding Growth. *Nanotechnology* **2008,** *19*, 175603.

25. Choi, H.; Chen, W. T.; Kamat, P. V. K., Know Thy Nano Neighbor. Plasmonic versus Electron Charging Effects of Metal Nanoparticles in Dye-Sensitized Solar Cells. *ACS Nano* **2012,** *6* (5), 4418–4427.

26. E308-01, Standard Practice for Computing the Colors of Objects by Using the CIE System. American Society for Testing and Materials (ASTM): 2001.

27. Dehn, M. H.; Arseneau, D. J.; Buck, T.; Cortie, D. L.; Fleming, D. G.; King, S. R.; MacFarlane, W. A.; McDonagh, A. M.; McFadden, R. M. L.; Mitchell, D. R. G.; Kie, R. F., Nature of magnetism in thiol-capped gold nanoparticles investigated with Muon Spin Rotation. *Appl. Phys. Lett.* **2018**, in press.

28. Malola, S.; Lehtovaara, L.; Enkovaara, J.; Häkkinen, H., Birth of the Localized Surface Plasmon Resonance in Monolayer-Protected Gold Nanoclusters. *ACS Nano* **2013,** *7* (11), 10263–10270.

29. Martin, J. E.; Odinek, J.; Wilcoxon, J. P.; Anderson, R. A.; Provencio, P., Sintering of Alkanethiol-Capped Gold and Platinum Nanoclusters. *J. Phys. Chem. B* **2003,** *107* (2), 430–434.

30. Pellegrini, G.; Mattei, G.; Bello, V.; Mazzoldi, P., Interacting Metal Nanoparticles: Optical Properties from Nanoparticle Dimers to Core-Satellite Systems. *Mater. Sci. Eng. C* **2007,** *27* (5-8), 1347–1350.

31. Peceros, K. E.; Xu, X.; Bulcock, S. R.; Cortie, M. B., Dipole-dipole plasmon interactions in gold-on-polystyrene composites. *J. Phys. Chem. B* **2005,** *109* (46), 21516-21520.

32. Babar, S.; Weaver, J. H., Optical constants of Cu, Ag, and Au revisited. *Appl. Opt.* **2015,** *54* (3), 477-481.

33. Gupta, A.; Mandal, S.; Katiyar, M.; Mohapatra, Y. N., Film processing characteristics of nano gold suitable for conductive application on flexible substrates. *Thin Solid Films* **2012,** *520*, 5664-5670.

34. Hansen, T. W.; Delariva, A. T.; Challa, S. R.; Datye, A. K., Sintering of catalytic nanoparticles: Particle migration or Ostwald ripening? *Acc. Chem. Res.* **2013,** *46* (8), 1720–1730.

35. Bore, M. T.; Pham, H. N.; Switzer, E. E.; Ward, T. L.; Fukuoka, A.; Datye, A. K., The Role of Pore Size and Structure on the Thermal Stability of Gold Nanoparticles within Mesoporous Silica. *J. Phys. Chem. B* **2005,** *109*, 2873-2880.

36. Thompson, C. V., Solid-State Dewetting of Thin Films. *Annu. Rev. Mater. Res.* **2012,** *42* (1), 399–434.

37. Chen, Y.; Palmer, R. E.; Wilcoxon, J. P., Sintering of Passivated Gold Nanoparticles under the Electron Beam. *Langmuir* **2006,** *22* (6), 2851–2855.

38. Eustis, S.; El-Sayed, M. A., Why Gold Nanoparticles Are More Precious than Pretty Gold: Noble Metal Surface Plasmon Resonance and Its Enhancement of the Radiative and Nonradiative Properties of Nanocrystals of Different Shapes. *Chem. Soc. Rev.* **2006,** *35* (3), 209–217.

39. Presland, A. E. B.; Price, G. L.; Trimm, D. L., Kinetics of Hillock and Island Formation during Annealing of Thin Silver Films. *Prog. Surf. Sci.* **1972,** *3* (1), 63–96.

40. Ingham, B.; Lim, T. H.; Dotzler, C. J.; Henning, A.; Toney, M. F.; Tilley, R. D., How nanoparticles coalesce: an in situ study of Au nanoparticle aggregation and grain growth. *Chem. Mater* **2011,** *23* 3312–3317.

SYNOPSIS TOC